Switching Behavior of Graphene Nanoribbon FETs

1st Mathias Pech
Chair for Communication Technology
TU Dortmund
Dortmund, Germany
mathias.pech@tu-dortmund.de

2nd Dirk Schulz
Chair for Communication Technology
TU Dortmund
Dortmund, Germany
dirk2.schulz@tu-dortmund.de

2024 International Conference on Simulation of Semiconductor Processes and Devices (SISPAD) | 979-8-3315-1635-2/24/$31.00 ©2024 IEEE | DOI: 10.1109/SISPAD62626.2024.10732903

Abstract—An efficient model capable of the time-resolved modeling of armchair graphene nanoribbon field-effect transistors based on a Wigner Transport Equation with non-parabolic corrections is presented. With the inclusion of a mode-space approach the computational burden is heavily reduced. The resulting charge carrier and current densities agree well with those obtained through a real space tight-binding formulation of a non-equilibrium Greens Function method in the stationary case. The self-consistent and transient capabilities of our proposed approach are demonstrated for the THz switching behavior. Furthermore, the presented method is well suited for the analysis of nanotubes or nanoribbons composed of different materials, as well as for the extension to interband transport.

Index Terms—Graphene nanoribbon, Wigner transport equation, Quantum transport, DGFET, Switching

I. Introduction

In order to continue the scaling of nanoelectronic devices, field-effect transistors (FETs) based on 1D materials such as nanotubes and nanoribbons are promising options [1]. Two of the most well known candidates are carbon nanotubes (CNTs) and graphene nanoribbons (GNRs) which can, depending on chirality, edge configuration and width offer high charge carrier mobilities and band gaps similar to those of conventional semiconductors, as well as a plethora of other potentially exploitable transport phenomena [2] that make them suitable for THz applications [3]. Even though issues with large-scale integration still persist, the research into possible applications remains ongoing and as such requires the simulation of the quantum charge carrier transport.

For the devices mentioned, the empirical tight-binding method offers itself as an easy to implement approach in both real and mode space and is readily incorporated into transport models based on non-equilibrium Greens functions (NEGF) [4] and density matrices [5]. However, models based on the effective mass approximation can be a valid and computationally efficient alternative if the non-parabolicity corrections of the energy dispersion are included [4].

On account of the computational effort, the NEGF formalism is mostly limited to the stationary case so that the Wigner Transport equation (WTE) is chosen for the analysis of the time-resolved quantum charge carrier transport in GNR FETs. Therefore, a previously presented approach of a phase space exponential operator for the WTE [6], [7] is extended to include the necessary non-parabolic corrections by means of a power series expansion of the Hamiltonian to the order of ∇^4.

II. Phase Space Exponential Operator for the Non-parabolic Wigner Transport Equation

Assuming a constant effective mass along the channel, the device Hamiltonian can be written as [8]

$$\hat{\mathcal{H}} = \sum_{n=1} \hbar^{2n} c_{2n} \nabla^{2n} + V(\boldsymbol{r}) \tag{1}$$

with the coefficients c_{2n} including the respective effective masses. Assuming transport along one dominant direction and taking only first order corrections into account (1) simplifies to

$$\hat{\mathcal{H}} = \hbar^4 c_4 \frac{\partial^4}{\partial x^4} + \hbar^2 c_2 \frac{\partial^2}{\partial x^2} + V(\boldsymbol{x}). \tag{2}$$

After inserting (2) into the von-Neumann equation and applying the inverse Weyl transform, one arrives at the WTE for the Wigner function $f(\chi, k, t)$ given by [8]

$$\begin{aligned} \frac{\partial}{\partial t} f(\chi,k,t) &= \hbar^3 c_4 k \frac{\partial^3}{\partial \chi^3} f(\chi,k,t) \\ &\quad + \left(-4\hbar^3 c_4 k^3 + \hbar c_2 k\right) \frac{\partial}{\partial \chi} f(\chi,k,t) \\ &\quad + \frac{1}{\imath\hbar} \int \frac{dk'}{2\pi} \tilde{V}(\chi, k-k') f(\chi,k',t) \end{aligned} \tag{3}$$

with the integral kernel [7]

$$\tilde{V}(\chi,k) = \int d\xi \exp(-\imath k\xi) \cdot \bar{V}, \tag{4}$$

where the term

$$\bar{V}(\chi,\xi) = V\left(\chi + \frac{\xi}{2}\right) - V\left(\chi - \frac{\xi}{2}\right) - \imath W(\xi) \tag{5}$$

contains the band potential, the self-consistent Hartree potential and any externally applied biases (V), as well as the complex absorbing potential $\imath W$, which accounts for the finite computational domain in ξ-direction [9]. At this point, the k-direction is readily discretized into N_k equidistant points so that the vector $\boldsymbol{f}(\chi,t)$ contains all discrete k values, leading to the semi-discrete WTE

$$\frac{\partial}{\partial t}\boldsymbol{f}(\chi,t) = [D_3] \frac{\partial^3}{\partial \chi^3}\boldsymbol{f}(\chi,t) + [D_1] \frac{\partial}{\partial \chi}\boldsymbol{f}(\chi,t) + [D_0]\, \boldsymbol{f}(\chi,t) \tag{6}$$

with the matrix elements

$$\begin{aligned} D_3^{l,l'} &= \hbar^3 c_4 k_l \delta_{l,l'} \\ D_1^{l,l'} &= \left(-\hbar^3 c_4 k_l^3 + \hbar c_2 k_l\right) \delta_{l,l'} \\ D_0^{l,l'} &= \frac{1}{\imath\hbar}\frac{\Delta_k}{2\pi}\sum_{j=1}^{N_\xi} \Delta_\xi \exp\left(-\imath\left(k_l - k_l'\right)\xi_j\right) \bar{V}(\chi, \xi_j), \end{aligned} \tag{7}$$

where the integral from (4) was approximated by utilizing the midpoint rule [7].

Next, the derivatives in χ-direction are to be discretized. Accordingly, the phase space exponential integrator method from [6], [7] has to be extended to allow for the inclusion of higher order derivatives in χ. After rewriting the right-hand side of (6) as a system of first order coupled differential equations

$$\frac{\partial}{\partial\chi}\mathbf{\Pi}(\chi) = \mathbf{\Pi}(\chi)\left[\mathbf{\Gamma}\right] \tag{8}$$

with

$$\mathbf{\Pi}(\chi) = \left(\boldsymbol{f}(\chi), \frac{\partial}{\partial\chi}\boldsymbol{f}(\chi), \frac{\partial^2}{\partial\chi^2}\boldsymbol{f}(\chi)\right)^T \tag{9}$$

and

$$[\mathbf{\Gamma}] = \begin{bmatrix} [0] & [\mathbb{1}] & [0] \\ [0] & [0] & [\mathbb{1}] \\ -[D_3]^{-1}[D_0] & -[D_3]^{-1}[D_1] & [0] \end{bmatrix} \tag{10}$$

where $[\mathbb{1}]$ contains the unity matrix, (8) can be solved analytically by use of an exponential integrator. After applying the mid-point rule again, a propagation algorithm is achieved [7]:

$$\mathbf{\Pi}(\chi_{i+1}) = \exp\left(\left[\mathbf{\Gamma}(\chi_{i+\frac{1}{2}})\right]\Delta_\chi\right)\mathbf{\Pi}(\chi_i). \tag{11}$$

To reduce the computational burden, the matrix exponential in (11) is approximated by utilizing the first order Padé approximant [7], [13], resulting in

$$\begin{aligned} &\left[[\mathbb{1}] - \left[\mathbf{\Gamma}(\chi_{i+\frac{1}{2}})\right]\frac{n\cdot\Delta_\chi}{2}\right]\mathbf{\Pi}(\chi_{i+n}) \\ &\qquad = \left[[\mathbb{1}] + \left[\mathbf{\Gamma}(\chi_{i+\frac{1}{2}})\right]\frac{n\cdot\Delta_\chi}{2}\right]\mathbf{\Pi}(\chi_i), \end{aligned} \tag{12}$$

with n indicating the times the matrix exponential is applied. In order to find a closed formulation for all derivatives in (6), (12) is evaluated for $n = 1, 2, 3$. By evaluating each row of (12) by itself, nine equations are obtained which can be inserted into each other. After a lengthy calculation and the introduction of the abbreviation $\boldsymbol{f}(\chi_i) = \boldsymbol{f}_i$ the novel approximation of the third order derivative in χ is obtained

$$\frac{\partial^3}{\partial\chi^3}\boldsymbol{f}(\chi)\Big|_{\chi_{i+\frac{1}{2}}} \rightarrow \frac{-\boldsymbol{f}_{i-2} + \boldsymbol{f}_{i-1} + 2\boldsymbol{f}_i - 2\boldsymbol{f}_{i+1} - \boldsymbol{f}_{i+2} + \boldsymbol{f}_{i+3}}{4\Delta_\chi^3}, \tag{13}$$

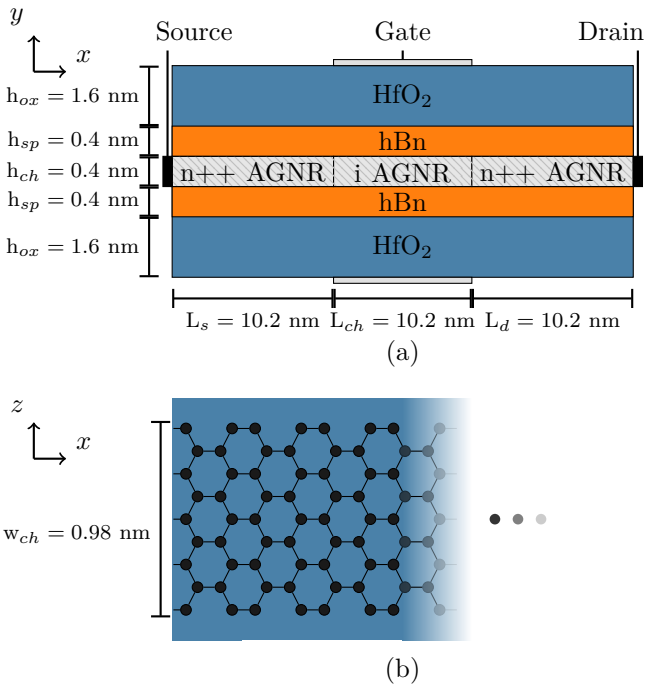

Fig. 1. Schematic of the 9-AGNR-FET in the xy-plane (a) and xz-plane (b).

in addition to the previously known terms from [7] for the approximation of the first order derivative and zeroth order term given by:

$$\begin{aligned} \frac{\partial}{\partial\chi}\boldsymbol{f}(\chi)\Big|_{\chi_{i+\frac{1}{2}}} &\rightarrow \frac{-\boldsymbol{f}_i + \boldsymbol{f}_{i+1}}{\Delta_\chi}, \\ \boldsymbol{f}(\chi)\Big|_{\chi_{i+\frac{1}{2}}} &\rightarrow \frac{\boldsymbol{f}_i + \boldsymbol{f}_{i+1}}{2}. \end{aligned} \tag{14}$$

After inserting (13) and (14) into (6), one arrives at the final discrete formulation of the WTE including the first order non-parabolic corrections:

$$\begin{aligned} &\frac{\partial}{\partial t}\frac{\boldsymbol{f}_i + \boldsymbol{f}_{i+1}}{2} \\ &\quad = [D_3]\cdot\frac{-\boldsymbol{f}_{i-2} + \boldsymbol{f}_{i-1} + 2\boldsymbol{f}_i - 2\boldsymbol{f}_{i+1} - \boldsymbol{f}_{i+2} + \boldsymbol{f}_{i+3}}{4\Delta_\chi^3} \\ &\quad + [D_1]\cdot\frac{-\boldsymbol{f}_i + \boldsymbol{f}_{i+1}}{\Delta_\chi} + [D_0(\chi_{i+\frac{1}{2}})]\cdot\frac{\boldsymbol{f}_i + \boldsymbol{f}_{i+1}}{2}. \end{aligned} \tag{15}$$

After the formulation of (15) for all $\boldsymbol{f}_1, \boldsymbol{f}_2, ..., \boldsymbol{f}_{N_\chi}$ the right-hand side of the WTE can be rewritten as a system matrix [7], [13] which is the basis for all further calculations.

III. Analysis of charge carrier transport in armchair GNR FETs

A schematic of the armchair GNR (AGNR) FET with the most relevant device parameters is shown in Fig. 1. For the carbon-carbon bonds a distance of $a_{cc} = 0.142$ nm with nearest neighbor hopping energy of $t = 2.7$ eV and

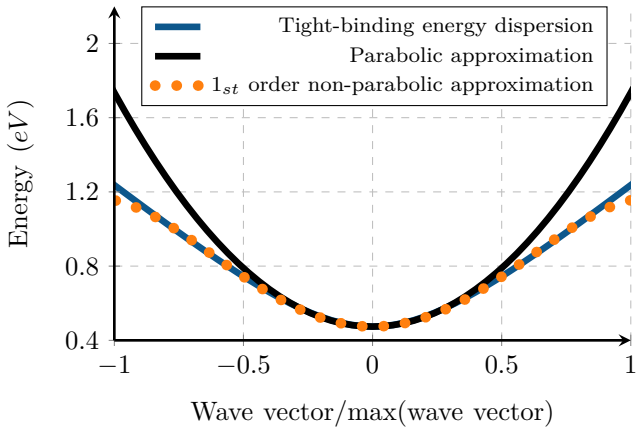

Fig. 2. The energy dispersion obtained by a nearest neighbor tight-binding Hamiltonian is approximated well with the first order non-parabolic correction from (2) for up to $k = k_{max} = \pi/(12 \cdot a_{cc})$, i.e. one quarter of the distance from Γ to X, whereas the parabolic approximation deviates significantly.

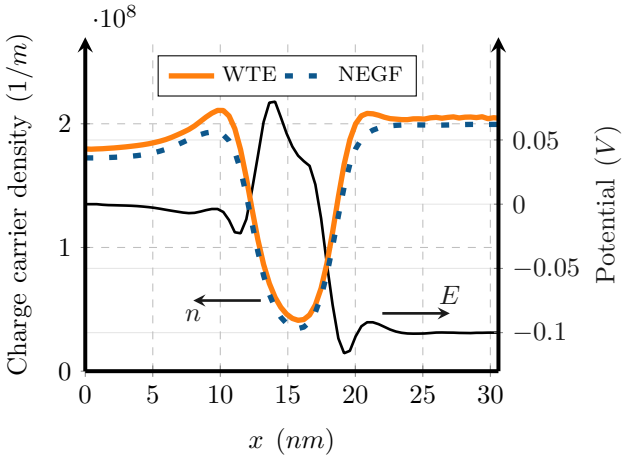

Fig. 3. The charge carrier densities obtained through the Wigner Transport Equation with non-parabolic corrections agree reasonably well with those of a real space NEGF approach for the same potential.

0 for all other neighbors is used with the effects of edge bond relaxation being neglected for the sake of simplicity.

The FET consists of a 9-AGNR layer that is located between two HfO_2 films with one layer of hBn in between as suggested in [10] and controlled via a dual-gate for which matched work functions are assumed. The relative permittivities of the AGNR channel, hBn and HfO_2 films are given by $\epsilon_{r,\mathrm{GNR}} = 2.5$, $\epsilon_{r\mathrm{hBn}} = 4$ and $\epsilon_{r\mathrm{HfO_2}} = 24$, respectively [10]. A fraction of $19 \cdot 10^{-4}$ dopants/carbon atoms is assumed in the drain and source regions.

The coefficients c_2 and c_4 from (2) are obtained by fitting to the energy dispersion shown in Fig. 2 which is calculated by solving for the eigenenergies of the device Hamiltonian, resulting in $c_4 = -5.379 \cdot 10^{49} \cdot m_0^{-1}$ and $c_2 = 4.663 \cdot m_0^{-1}$ for the non-parabolic approximation, $c_4 = 0$ and $c_2 = 4.868 \cdot m_0^{-1}$ for the parabolic case and a band gap of $E_G = 0.948$ eV.

In terms of self-consistency, the charge carrier transport and Poisson's equation are solved iteratively until the Hartree potential of subsequent iteration converges. For the transient case, the WTE and Poisson's equation are solved once per time-step. In order to reduce the computational effort, the charge carrier transport is calculated in the xz plane with the assumption of a constant electrical potential in z-direction. The resulting charge carrier densities are then inserted into Poisson's equation which is solved in the xy plane using a finite-difference scheme. Ballistic charge carrier transport and room temperature operation are assumed in all cases

For the WTE, a mode-space approach [11] is utilized, heavily reducing the computational burden. Because Poisson's equation is solved in the xy plane, the subband profiles are not needed explicitly and are therefore not calculated. Thus, only the boundary conditions in addition to the potential term are modified with the subband energy (i.e. half of E_G) being added to the latter. Only the first conduction subband lowest in energy and closest to the Fermi level is taken into account. Inflow boundary conditions [12] are assumed at the source and drain contacts. For the time-resolved simulations, the time derivative on the left-hand side of (15) can also be expressed in terms of an exponential integrator which is then approximated by the application of a Crank-Nicolson scheme [13]. A discretization width of $\Delta_x = 3a_{cc}$ is used in transport direction with $N_k = 260$ equidistant values in phase space between ± 2.6 nm^{-1}. A time step width of $\Delta_t = 2$ fs is used for the transient case.

Regarding the reference approach a real space tight-binding NEGF method is employed in the xz plane [4]. A lopez sancho algorithm is used to massively speed up the calculation of the surface energies at the contacts [14]. Because Poisson's equation is solved on the same discretization points in x as the WTE, the potential used in applying the NEGF is interpolated where necessary.

IV. Results

The charge carrier densities for an exemplary potential obtained by the WTE and reference approach are shown in Fig. 3. The results are in good agreement, with the additional benefit of computation times for the WTE being less than one hundredth of those of the NEGF approach. Minor deviations occur naturally due to the uncoupled mode space approximation that is used, as well as the difference in the treatment of device boundaries in the WTE and NEGF approaches. The self-consistent drain-end current as a function of the drain-source voltage is shown in Fig. 4 for three different gate voltages along with the flatband case, where the potential difference between source and drain is assumed to decrease linearly in the channel region. As it can be seen, the results converge well and resemble those of conventional quantum confined dual-gate FETs. To analyze the time-resolved switching behavior, the device is modified to $L_s = L_d = 13.6$ nm and

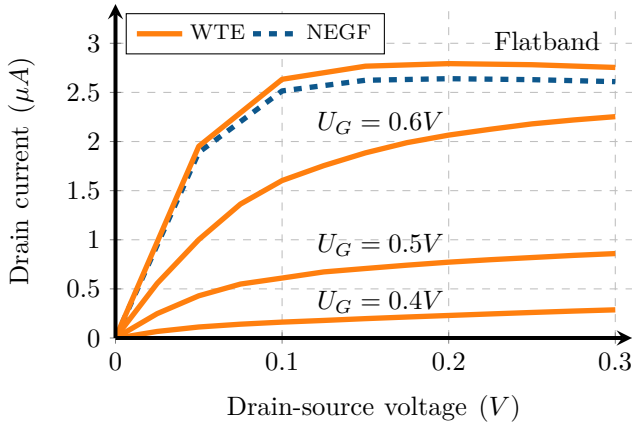

Fig. 4. The self-consistent drain-end current densities are shown for three different gate voltages U_G. In addition, results for the flatband case are compared to those of a NEGF approach, where issues with convergence arose for the self-consistent case, likely because of the mismatch between real space charge carrier densities and Hartree calculations on a uniform grid.

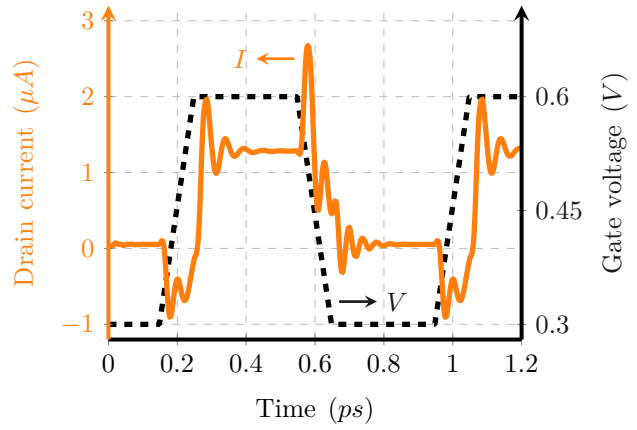

Fig. 5. The self-consistent time dependent drain-end current shows significant overshoot effects during the switching process.

$L_{ch} = 6.8$ nm and the permittivities are increased towards the contact to reduce issues with the self-consistency at the contacts. A square signal between 0.3 V and 0.6 V is applied to the gate contact with a cycle length of 0.8 ps and 50 % duty cycle. To improve the accuracy of the results, a finite slew rate of 3 V/ps is applied [15]. The transient evolution of the drain-end current is shown in Fig. 5. As it can be observed, an overshoot effect occurs both during on and off switching with the peak drain current exceeding the steady state current by roughly two times. The steady state drain-end current is reached after about 200 fs in both cases.

V. Summary

The phase-space exponential operator scheme for the WTE has been extended to take energy band non-parabolicity into account. By comparison to reference results it is shown that it can readily be applied onto devices such as AGNR FETs to model the self-consistent stationary and time-resolved behavior where drain-end current overshoot is observed during switching processes.

Acknowledgment

This work was supported by the Deutsche Forschungsgemeinschaft DFG (Grant SCHU 1016/8). Computing time was provided on the LiDO3 cluster, partially funded in the course of the Large-Scale Equipment Initiative by the DFG as project 271512359.

References

[1] F. Schwierz, "Graphene transistors." Nature nanotechnology, vol. 5 7, pp. 487–96, 2010.
[2] S. Dubois, Z. Zanolli, X. Declerck, and J.-C. Charlier, "Electronic properties and quantum transport in graphene-based nanostructures," The European Physical Journal B, vol. 72, pp. 1–24, 11 2009.
[3] M. Portnoi, O. Kibis, and M. Rosenau da Costa, "Terahertz applications of carbon nanotubes," Superlattices and Microstructures, vol. 43, no. 5, pp. 399–407, 2008, proceedings of the 7th International Conference on Physics of Light-Matter Coupling in Nanostructures.
[4] R. Grassi, S. Poli, E. Gnani, A. Gnudi, S. Reggiani, and G. Baccarani, "Tight-binding and effective mass modeling of armchair carbon nanoribbon fets," in 2008 9th International Conference on Ultimate Integration of Silicon, 2008, pp. 121–124.
[5] A. Abdi, M. Pech, and D. Schulz, "Incorporation of the tight binding hamiltonian into quantum liouville-type equations," in International Workshop on Computational Nanotechnology (IWCN), 2023.
[6] D. Schulz and A. Mahmood, "Approximation of a phase space operator for the numerical solution of the wigner equation," IEEE Journal of Quantum Electronics, vol. 52, no. 2, pp. 1–9, 2016.
[7] L. Schulz and D. Schulz, "Formulation of a phase space exponential operator for the wigner transport equation accounting for the spatial variation of the effective mass," Journal of Computational Electronics, vol. 19, 2020.
[8] K.-Y. Kim and B. Lee, "Wigner function formulation in non-parabolic semiconductors using power series dispersion relation," Journal of Applied Physics, vol. 86, no. 9, pp. 5085–5093, 1999.
[9] L. Schulz and D. Schulz, "Complex absorbing potential formalism accounting for open boundary conditions within the wigner transport equation," IEEE Transactions on Nanotechnology, vol. 18, pp. 830–838, 2019.
[10] H. Sarvari, R. Ghayour, and E. Dastjerdy, "Frequency analysis of graphene nanoribbon fet by non-equilibrium green's function in mode space," Physica E: Low-dimensional Systems and Nanostructures, vol. 43, no. 8, pp. 1509–1513, 2011.
[11] R. Venugopal, Z. Ren, S. Datta, M. S. Lundstrom, and D. Jovanovic, "Simulating quantum transport in nanoscale transistors: Real versus mode-space approaches," Journal of Applied Physics, vol. 92, no. 7, pp. 3730–3739, 2002.
[12] W. R. Frensley, "Boundary conditions for open quantum systems driven far from equilibrium," Rev. Mod. Phys., vol. 62, pp. 745–791, Jul 1990.
[13] L. Schulz, B. Inci, M. Pech, and D. Schulz, "Subdomain-based exponential integrators for quantum liouville-type equations," Journal of Computational Electronics, vol. 20, no. 6, pp. 2070–2090, 2021.
[14] M. P. L. Sancho, J. M. L. Sancho, J. M. L. Sancho, and J. Rubio, "Highly convergent schemes for the calculation of bulk and surface green functions," Journal of Physics F: Metal Physics, vol. 15, no. 4, p. 851, apr 1985.
[15] B. Biegel and J. Plummer, "Applied bias slewing in transient wigner function simulation of resonant tunneling diodes," IEEE Transactions on Electron Devices, vol. 44, no. 5, pp. 733–737, 1997.